Scientia Iranica F (2018) 25(3), 1879–1890

SCIENTIA IRANICA

Sharif University of Technology
Scientia Iranica
Transactions F: Nanotechnology
http://scientiairanica.sharif.edu

Molecular dynamics simulation: The effect of graphene on the mechanical properties of epoxy based photoresist: SU8

F. Mohammadzadeh Honarvar[a], B. Pourabbas[a*], M. Salami Hosseini[a], M. Kharazi[b], and H. Erfan-Niya[c]

a. *Department of Polymer Engineering, Nanostructured Materials Research Centre, Sahand University of Technology, Sahand New Town, Tabriz, Iran.*
b. *Department of Mechanical Engineering, Sahand University of Technology, Sahand New Town, Tabriz, Iran.*
c. *Department of Chemical and Petroleum Engineering, University of Tabriz, Tabriz, Iran.*

Received 5 December 2017; received in revised form 24 February 2018; accepted 5 May 2018

KEYWORDS
SU8;
Graphene;
Nanocomposite;
Mechanical properties;
Molecular dynamics.

Abstract. SU8 is an epoxy-Novolac resin that is used as a photo initiator in micro- and nano-fabrication techniques. From literature, graphene has been shown to result in a significant improvement in the properties of the composites. However, due to the nanometer size of the graphene layers, there is no experimental tool to obtain some insight into the fillers inside the resin, especially when the materials are under mechanical deformations where simulation techniques work well. Therefore, SU8 and SU8-graphene nanocomposites as the model compounds were taken to be investigated by an atomistic molecular dynamic approach to demonstrate the effect of graphene layers. This leads to mechanical property enhancement such as Young's, bulk and shear modules affected by the aspect ratio of the graphene layers; high-aspect ratio graphene in SU8 leads to an 81% improvement in Young's, 100% in bulk, and 83% in shear moduli, in addition to higher density and less graphene wrinkling.

1. Introduction

The resin with the commercial name SU8 is an epoxy-Novolac resin used mainly as a negative sub-micron resolution photoresist in lithographic processes. The properties of SU8, such as rigidity, low toxicity, transparency to visible light, high thermal and chemical stability, low cost, and simplicity of the process, have led to its broad range of applications in micro- and nano-fabrications. Sensors, micro lenses, optical devices, etched resist masks, micro fluidics, and Micro Electro Mechanical Systems (MEMS) are just examples of many devices in which SU8 can be used in one or more steps of production [1-9].

Recently, researchers have managed to alternate the properties of nano-filled polymers (electrical, optical, thermal, mechanical, rheological, barrier, etc.) using different available Nano-sized Particles (NPs) as the filler. As a matter of fact, only a small weight percentage of the fillers, in contrast to traditional composites, can be enough for a major improvement in the properties [10-13]. Nanoclays, silica nanoparticles, Carbon Nano Tubes (CNTs), and other carbon-

*. *Corresponding author. Tel.: +98 41 3344 9083; Fax: +98 41 3344 4303*
E-mail addresses: f_mohamadzadeh@sut.ac.ir (F. Mohammadzadeh Honarvar); pourabas@sut.ac.ir (B. Pourabbas); salami@sut.ac.ir (M. Salami Hosseini); kharazi@sut.ac.ir (M. Kharazi); herfan@tabrizu.ac.ir (H. Erfan-Niya).

doi: 10.24200/sci.2018.5697.1432

based particles, including diamantes and single-layer graphene layers, are amongst the widely used NPs used for newly developed materials and nanocomposites [14-17]. Outstanding properties are reported for graphene-polymer nanocomposites [11,18,19]; however, from an experimental standpoint, there is not any instrumental method for investigating the real stories of the nanometric-scale interactions of the materials remaining as a big challenge. Though many experimental methods have been developed for probing purposes at the finer scale of the materials, related knowledge, undoubtedly, is necessary for engineers to design new materials with desired properties without exceeding the number of the experimental trials [20]. To this end, several theoretical studies have studied graphene in polymeric nanocomposites using Molecular Dynamics (MD) simulation techniques [21-25]. This is indeed the hierarchical approach of the simulation or a multi-scale simulation hypothesis, describing how the macroscale properties can be predicted based on the data from the shorter scale of the lengths, i.e. the molecular dynamics. For instance, an atomistic MD simulation was employed by Skountzos et al. for graphene in PMMA in order to correlate the experimentally measured macro mechanical properties of the material with the atomistic scale interactions between the polymeric matrix and the filler [26]. As shown, functionalized graphene added to PMMA at very low content could lead to a very strong multi-functional material.

The multi-scale simulation concept was used by Ebrahimi et al. to compare how graphene or carbon nanotube is effective in the mechanical properties of Chitosan-based materials; related results showed that the graphene reinforcing effect was higher than the effect of carbon nanotubes [27].

Rahman and Haque studied graphene-epoxy nanocomposites in order to estimate the elastic constants using MD and Molecular Mechanic (MM) simulation methods. The methodology proved that, compared to Mori-Tanaka model, the results are in better accordance with the experimental data [28].

The method developed by Theodorou et al. and Rapold et al. provides a basic calculation and methodology for correlation and connectivity between the molecular-scale interactions and the macroscale properties in polymeric materials [29,30]. Based on this method, the system under simulation is subjected to a series of small strain deformations. Subsequently, the elastic constants are estimated theoretically from the second derivative of internal energy (U) with respect to the imposed strain. The method employed on atactic polypropylene showed acceptable results with the experimental data [31].

For the first time, SU8 and SU8-graphene nanocomposites are studied in the present work using a method put forward by Theodorou et al. and Rapold et al. This involves several MD simulation and mathematical steps leading to a realistic description of the interactions between the molecules of the components which results in the prediction of the macroscale mechanical properties. The simulation details and calculations of the mechanical property determination, in addition to graphical and numerical results, are provided in the following sections.

2. Simulation details

The commercial SU8 is a single-component product that consists of a multi-functional epoxy-Novolac resin, γ-butyrolactone as a reactive diluent, and a photoinitiator [32-34]. For the cured product, different densities have been reported varying from 1.05 to 1.19 g/cm^3 depending on the process conditions and composition [35-38]. From a structural point of view, the cured SU8 is a real three-dimensional network; therefore, the key point in the MD simulation is to find a substituted, yet smaller, structure to represent the real compound's properties. This was carried out by examining several suggested molecular structures using previously published works on the structural analysis of the cured SU8. In order to do this, results obtained by Jun Zhang et al. on the structural analysis of the cured SU8 and MD simulation done by Tam et al. were considered [32,38]. Zhang et al. fragmented the completely cured SU8 inside a mass spectrometer in order to depict a chemical structure for the cured SU8 network and determined different chemical fragments with population percentage. On the other hand, Tam simulated the cross-linking of SU8 using an effective dynamic algorithm under PCFF, CVFF, and Dreiding force fields. Ring opening polymerization without termination was the polymerization reaction considered for curing simulation. For the terminal atoms, hydrogens were substituted to achieve the saturation of the bonds. The final degree of cross-linking and density using PCFF force field were achieved to be 82.5% and 1.053 g/cm^3, respectively. Therefore, several structures were assembled, and the energy minimization process was performed for all of the suggested structures using PCFF force field with a cutoff distance of 8 Å at room temperature (298°K) until the total potential energy of each system reached its minimum state. The structure with the comparatively lowest potential energy was selected to be the representative structure of SU8 and was used in an MD simulation procedure. The representative structure is shown in Figure 1(a) and (b), consisting of the main structure of the original SU8 as the core, two free epoxy groups, and six epoxy groups reacted with γ-butyrolactone in a specific manner in order to resemble the cured SU8 as the model compound for simulation.

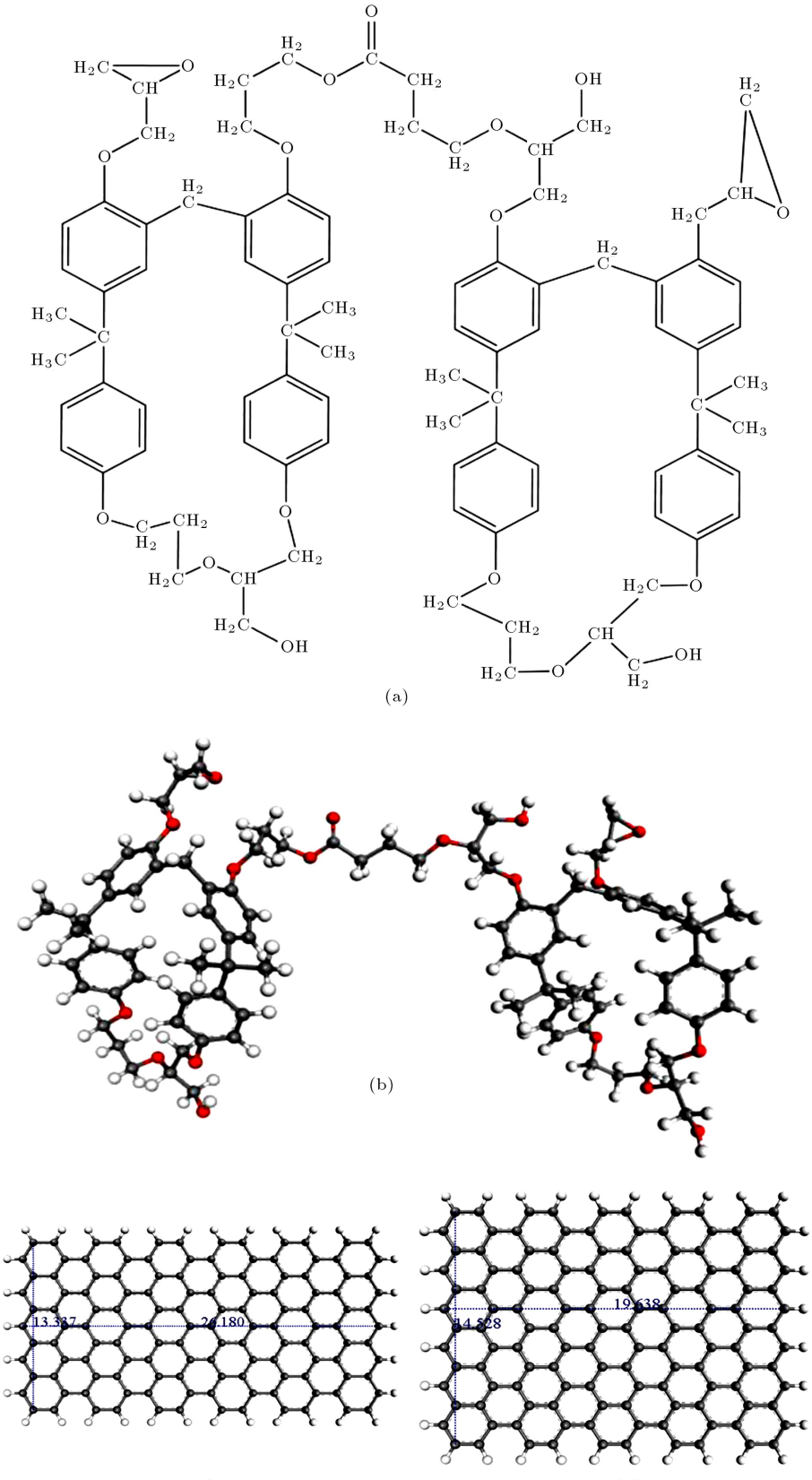

Figure 1. (a and b) The representative model SU8. (b) High-aspect ratio graphene (26.18 Å×13.337 Å). (c) Low-aspect ratio graphene (19.638×14.546 Å). Carbon, hydrogen, and oxygen atoms are demonstrated by gray, white, and red colored spheres, respectively.

For the nanocomposites, two types of graphenes with different aspect ratios were embedded in the simulation box including high-aspect ratio graphene (GH) (layer dimensions of: 26.18 Å × 13.337 Å) and low-aspect ratio graphene (GL) (layer dimensions: 19.638 Å × 14.546 Å) as shown in Figure 1(b) and (c), respectively.

Five model compounds were simulated for MD and mechanical property calculations: a simulation cell consisting of 50 model SU8 without graphene, 50 model SU8 with one or two high-aspect ratio graphenes, and 50 model SU8 with one or two low-aspect ratio graphenes. Thus, by inputting all of the atoms into the simulation cell, the weight percents of the garphene (low- and high-aspect ratios) in SU8/graphene nanocomposites are 2.1 or 4.2 wt.% (weight percent) depending on the number of graphene layers in the simulation cell. Table 1 summarizes the detailed constituents of each simulated compound, while Figure 2 shows the snapshot for the simulation cell for SU8-GH42.

The simulation procedure was performed on the simulation cell in periodic boundary conditions in all dimensions, and PCFF force field was employed to compute the atomic interactions within a cutoff distance of 8 Å. In order to bring about conformational stability for the system, simulation cells were subjected to 100000 steps of energy minimization followed by MD runs under an isobaric isothermal ensemble (NPT) without applying any external pressure at 298°K. This continued until the system reached the equilibrated state of energy, temperature, and density. The temperature and pressure were controlled by Nosé-Hoover thermostat-barostat algorithm [39,40]. For further equilibration, an isothermal isochoric ensemble (NVT) was performed on the system at 298°K. The system was analyzed for its energy, structure, and dynamics after the system had reached the new equilibrated state. The MD runs were performed for 2×10^6 steps of 0.1 fs and differential equations of motion were integrated using the velocity Verlet integrator [41,42] during the simulation run. Finally, the mechanical properties of SU8 and its nanocomposites were calculated based on the procedure previously developed by Theodorou [29]. Open-source code LAMMPS was used in all of the MD simulation steps described above [43].

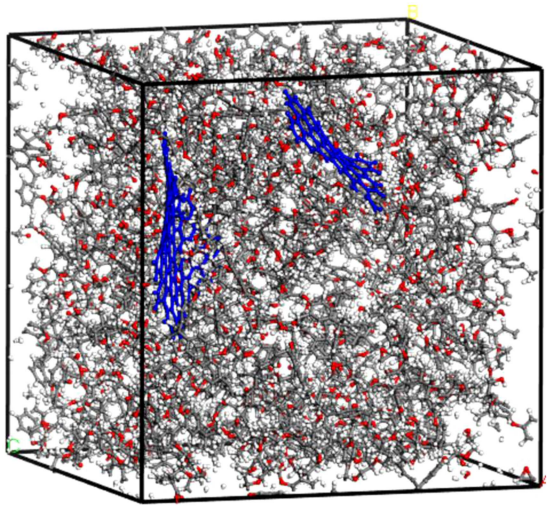

Figure 2. Snapshot of a typical nanocomposite simulation cell involving 50 model SU8 and two graphene layers (4.2 wt.%). Graphene layers are indicated by blue, but gray, white, and red colored spheres are carbon, hydrogen, and oxygen (in SU8), respectively.

The procedure for the mechanical property calculation and prediction is as follows:

1. First, performing energy minimization once again for the optimized configurations obtained from the previous MD runs to ensure the optimum geometry and minimum energy;
2. Applying strains (less than 1%);
3. Reoptimizing of the potential energy of the resulting structure;
4. Repeating steps 1 to 3 on the next optimized configuration from the MD run;
5. Averaging the mechanical properties over the data obtained for each configuration described above.

The elastic constants were calculated from the second derivative of internal energy (U) with respect to the imposed strain according to Eq. (1):

$$C_{ij} = \frac{1}{V}\frac{\partial^2 U}{\partial\varepsilon_i\partial\varepsilon_j} = \frac{\partial\sigma_i}{\partial\varepsilon_j}. \quad (1)$$

Table 1. Detailed explanation of the simulation strategy of the simulated SU8 and its graphene nanocomposites.

Notation	Number of the model SU8	Type of graphene	Number of graphene layers	Graphene wt.%
SU8	50	–	–	–
SU8-GL21	50	Low aspect ratio	1	2.1%
SU8-GL42	50	Low aspect ratio	2	4.2%
SU8-GH21	50	High aspect ratio	1	2.1%
SU8-GH42	50	High aspect ratio	2	4.2%

Lame constants (λ, μ) can be obtained from the elastic constants using Eqs. (2) and (3).

$$\lambda = \frac{1}{3}(C_{11} + C_{22} + C_{33}) - \frac{2}{3}(C_{44} + C_{55} + C_{66}), \quad (2)$$

$$\mu = \frac{1}{3}(C_{44} + C_{55} + C_{66}). \quad (3)$$

Now, the mechanical properties can be derived from the obtained Lame constants (Eqs. (4) to (6)):

$$E = \mu\frac{3\lambda + 2\mu}{\lambda + \mu}, \quad (4)$$

$$B = \lambda + \frac{2}{3}\mu, \quad (5)$$

$$G = \mu. \quad (6)$$

Detailed formulations and calculations are available in the literature [26,29].

3. Results and discussion

3.1. Structural properties

According to the procedures described above, the average density of the SU8 and SU8/graphene nanocomposites was calculated, as summarized in Table 2.

A range of experimental and theoretical values are reported in the literature for SU8 from 1.05 to 1.19 g/cm^3 [35-37]. Therefore, the predicted value for the pure SU8, which is indeed based on the model SU8 structure supposed in this work, is 1.108 ± 0.002 g/cm^3; acceptable agreement is observed. However, the predicted density for the nanocomposites with high-aspect ratio graphene is seen to be slightly higher than that for the pure SU8, while the nanocomposites with low-aspect ratio graphene show lower density. This obviously is related to the SU8 packing around the high-aspect ratio graphene layers leading to denser packing of the materials in simulated nanocomposite systems. In contrast, in the case of the low-aspect ratio graphene layers, orientation and packing of the SU8 molecules result in lower density of the materials around the layers. This, of course, can be verified by the radius of gyration R_g and an end-to-end distance of the SU8 molecules in the simulated systems. R_g versus probability density of the model SU8 is plotted in Figure 3, and the numerical values are reported in Table 3. It can be seen that graphene lowers R_g of the model SU8 molecules with respect to the pure SU8; however, this depends on the aspect ratio of the graphene layers in the system. The calculated Rg for the GL nanocomposites is 9.70 or 9.31 Å, while this is 8.81 or 9.01 Å for the GH nanocomposites. If R_g value of the pure SU8 be kept as the reference point 10.42 Å, lower R_g can be regarded as an indication of higher intra-molecular interactions (or lower inter-molecular interactions) with respect to the reference

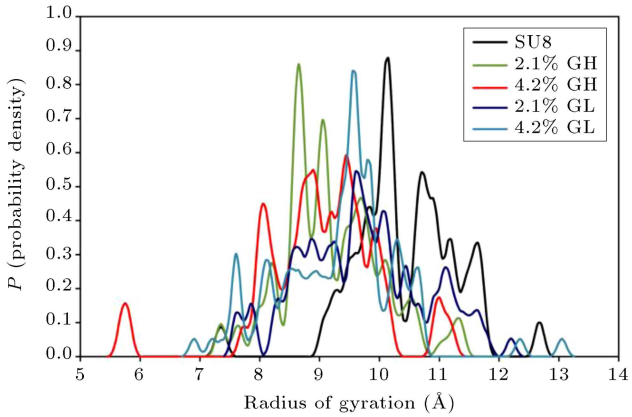

Figure 3. Radius of gyration (R_g) versus probability density for the model SU8 in the simulated systems.

Table 3. Calculated square end-to-end distance R^2 and average radius of gyration R_g for the model SU8 molecules in different systems.

System	R^2 (Å^2)	Average radius of gyration R_g (Å)
SU8	208.17	10.42
SU8-GH21	176.18	8.81
SU8-GH42	180.28	9.01
SU8-GL21	193.97	9.70
SU8-GL42	186.11	9.31

Table 2. Calculated density for the simulated systems at 298°K.

System	Predicted density (g/cm^3)	Experimental and/or theoretical values (g/cm^3)
SU8	1.088 ± 0.002	1.05 to 1.19 [35-37]
SU8-GH21	1.097 ± 0.004	N.A.
SU8-GH42	1.096 ± 0.003	N.A.
SU8-GL21	1.023 ± 0.005	N.A.
SU8-GL42	1.021 ± 0.003	N.A.

configuration (the pure SU8). In conclusion, high-aspect ratio graphene prevents inter-molecular interactions between SU8 molecules in a greater extent than the low-aspect graphene does. This can, of course, lead to two major conclusions. First, any inter-molecular interactions between graphene and SU8 cannot be a subject. Second, the graphene imposes its effect on surface area since the high-aspect ratio has greater surface area (698.325 Å^2) than the low-aspect ratio does (570.600 Å^2).

Useful results obtained from the MD simulation are the Radial Distribution Function (RDF) or element pair distribution functions which provide detailed information about the local packing and structural distribution over the length scale. The intra-molecular pair distribution reflects intra-molecular forces between the paired atoms belonging to the same molecule, and inter-molecular pairs in the same manner are the reflection of the interactions between atoms from different molecules. The RDF plots for atoms in the model for pure SU8 and the nanocomposites are shown in Figures 4 and 5.

In Figures 4 and 5, function $g_{\alpha-\beta}(r)$ is the length scale-dependent contribution function which shows atom α being in interaction with atom β both belonging to either the same molecule (intra-molecular) or different molecules (inter-molecular). For the inter-molecular interaction in Figure 4, $g_{\alpha-\beta}(r)$ approaches 1 at long distances obviously, because all the paired interactions lay within the sphere of infinite radius. However, for intra-molecular distribution in Figure 5, $g_{\alpha-\beta}(r)$ reaches zero at a long distance because atomic distribution for the atoms in a single molecule lay in a sphere with a certain volume. Function $g_{\alpha-\beta}(r)$, however, follows almost the same pattern for the pure SU8 and the nanocomposites, especially in the case of the intra-molecular distribution and shorter distances (Figure 5). The sharp hump or depression regions are, indeed, determined by the configurationally limitations including bond distance, angular rotations, temperature, and so on. If $g_{\alpha-\beta}(r)$ is compared with $g_{C-C}(r)$ for instance, for inter- and intra-molecular distributions, it can be concluded that $g_{\alpha-\beta}(r)$ values are different for different compounds, SU8, and the nanocomposites at a certain distance. Due to phenomenological properties of $g_{\alpha-\beta}(r)$, this can be attributed to different intermolecular and intra-molecular distributions in the specimens. As an example, $g_{C-C}(r)$ of the inter-molecular distribution (Figure 4) shows lower values for SU8-GL42 compared to the pure SU8 all over the length scales. This is while $g_{C-C}(r)$ of the intra-molecular distribution (Figure 5) for the same nanocomposite shows higher values with respect to the pure SU8. Therefore, knowing the fact

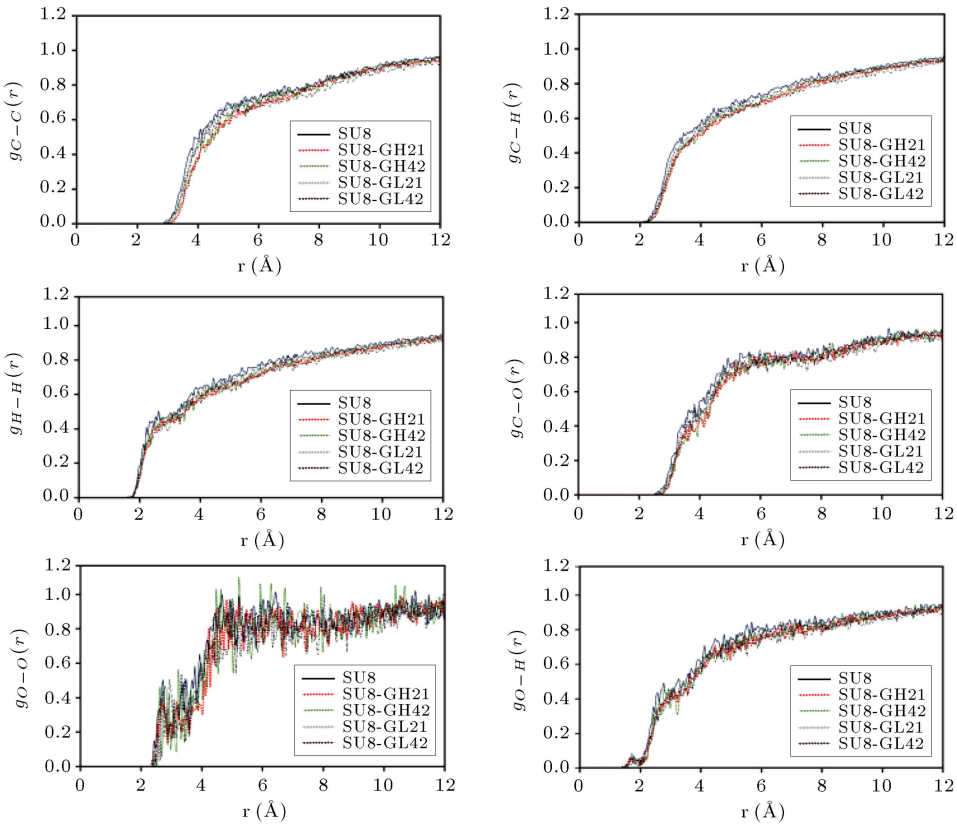

Figure 4. Inter-molecular Radial Distribution Function (RDF) for the paired atoms in the simulated systems: SU8, SU8GL21, SU8GL42, SU8GH21, and SU8GH42.

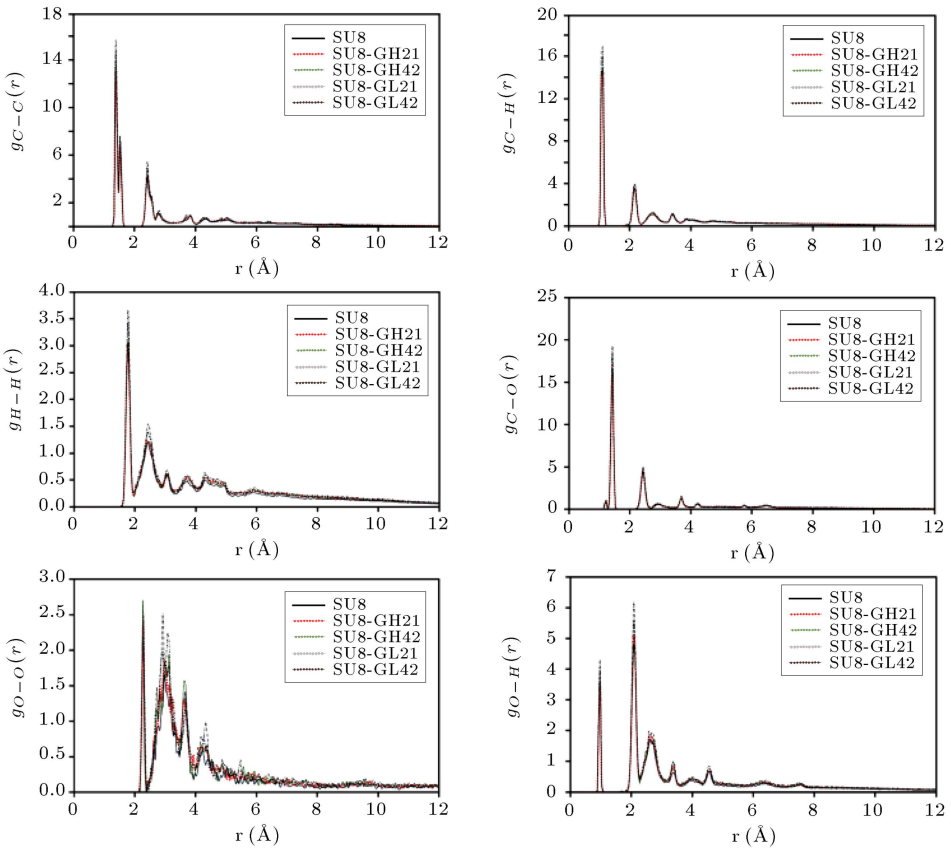

Figure 5. Intra-molecular Radial Distribution Function (RDF) for the paired atoms in the simulated systems: SU8, SU8GL21, SU8GL42, SU8GH21, and SU8GH42.

that inter-molecular or intra-molecular interactions are balanced in the most stable configuration, the paired atomic distribution function can be regarded as the function that provides information about the configuration and that how it is comparable in different conditions. In other words, a lower intra-molecular distribution deals with comparatively less effective inter-molecular interactions or higher intra-molecular interactions. The balanced intra- and inter-molecular interactions build the most stable configuration for the chain resulting in a characteristic R_g. Therefore, from the data in Table 3, the reason for reduced R_g of the nanocomposites with respect to the pure SU8 can be related to the graphene layer which, indeed, reduces the inter-molecular interactions of the SU8 molecules. Graphene layers apply this shielding effect through the surface so that high-aspect ratio graphenes with a higher surface area show comparatively lower R_g (Table 3). Additionally, in Figure 5, the absence of any periodical sharp peaks at distances greater than 4 Å and tending RDF to 1 provide proofs for the system being in amorphous morphology.

3.2. Graphene orientation

One major effect of inter-molecular interactions or tensile loads is the graphene deformation from its originally flat structure to a wrinkled or deformed state. It has been studied in several new works by molecular simulation techniques [44,45]. A planner atomic distribution profile is a tool that helps to understand where the graphene is located, what the orientation is, and that how the graphene is deformed inside the simulation cell. Figure 6 illustrates the relative atomic concentration planner profile along the three main simulation axes (001, 010, 001) for the nanocomposite containing 2.1 wt.% of GH or GL graphene, just after molecular stabilization and before any applied deformation load. Whether the graphene is a high- or low-aspect one, location, orientation, and deformation will be different as is clear on the concentration profiles and in snapshots given for each nanocomposite shown in Figure 6. High-aspect graphene in SU8-GH21 is lying supine alongside 'x' axes (100 plane) facing up 'y' axes (010 plane). This is while graphene in SU8-GL21 is almost standing alongside 'y' axes facing almost 'z' direction (001 plane). Though these are random positions, which can happen in any other conformation by successive MD simulations, the most important concern with the graphene layer within the nanocomposite is wrinkling or deformation. Relative atomic concentration shows plateau humps for high-aspect graphene in SU8-GH21 that appears as a sawtooth

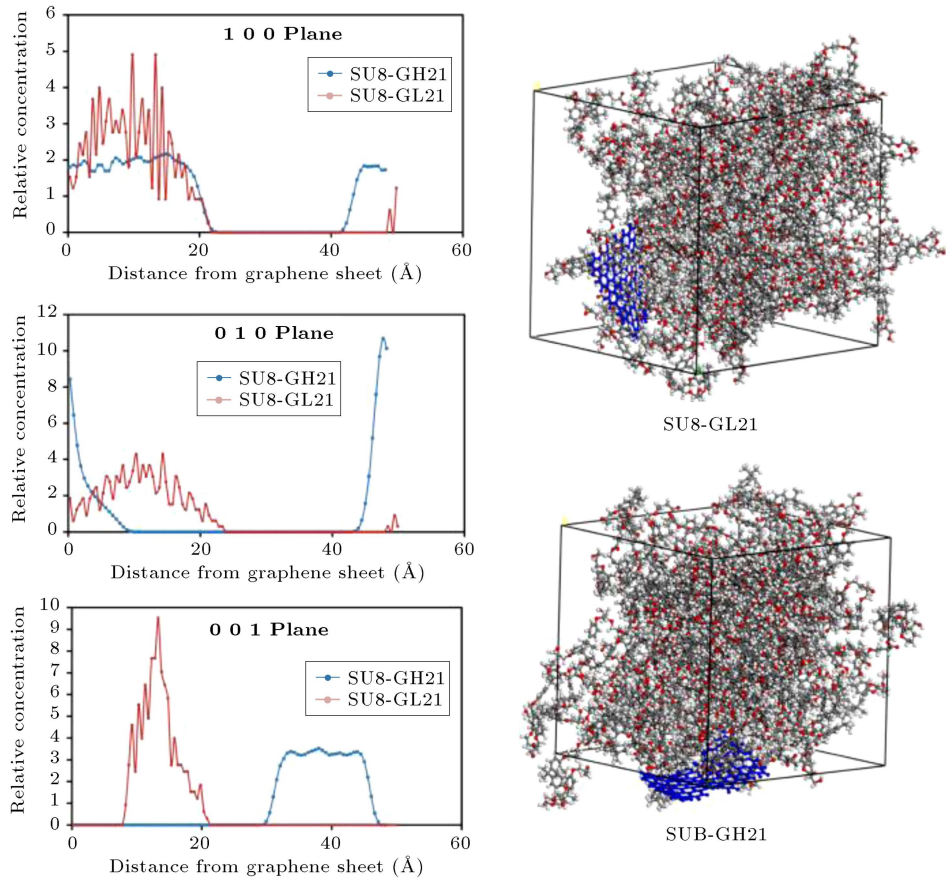

Figure 6. The relative atomic concentration planner profile along the three main simulation axes (001, 010, 001) for the nanocomposite containing 2.1 wt.% of GH or GL graphene.

mark in SU8-GL21, providing a proof that the low-aspect graphene is wrinkled alongside all the three axes of the simulation cell. This, of course, will affect the mechanical properties of the nanocomposites, discussed in the next section.

3.3. Mechanical properties

Mechanical properties of the simulated systems were predicted based on the methodology described earlier in Section 2. A constant strain was applied to the pure SU8 and to the nanocomposites. Any structural symmetry was removed from the system and, then, re-optimized, if necessary, to the lowest energy level. At the end of the process, the mechanical properties were calculated by averaging the quantitative parameters, as described earlier. The normalized calculated mechanical properties (Young, shear, and bulk moduli) are listed in Table 4.

Data in Table 4 are also compared graphically in Figures 7 to 9. As the first conclusion, incorporating graphene into the SU8 enhances the mechanical properties of the nanocomposites with respect to the pure SU8. For instance, Young, bulk and shear moduli in SU8-GH21 are increased to 63%, 202%, and 82%,

Table 4. Normalized mechanical properties (Young, shear and bulk modulus) for the model SU8 and its nanocomposites.

Sample	Normalized value		
	Young modulus	**Bulk modulus**	**Shear modulus**
SU8	1.000 ± 0.039	1.00 ± 0.010	1.000 ± 0.013
SU8-GH21	1.631 ± 0.075	2.017 ± 0.012	1.820 ± 0.020
SU8-GH42	1.807 ± 0.075	2.165 ± 0.018	1.832 ± 0.014
SU8-GL21	1.169 ± 0.076	1.283 ± 0.026	1.160 ± 0.028
SU8-GL42	1.361 ± 0.081	1.591 ± 0.015	1.483 ± 0.015

respectively, with respect to the pure SU8. Moreover, due to the increased weight percent of graphene in SU8-GH42, the mechanical properties can be seen that are increased even more up to 81%, 216%, and 83%.

However, high-aspect ratio graphene in the nanocomposites shows higher reinforcement effect, as is clear in Table 4, or comparative graphical demonstrations in Figures 7 to 9. This can be related to the density of the nanocomposites given in the preceding sections based on the density of the nanocomposites and being dependent on the aspect ratio of the graphene. In other words, relatively lower moduli for the compounds with low-aspect ratio graphene, in SU8-GL21 and SU8-GL42, result from the lower materials packing or lower density of the compounds. For instance, if the bulk modulus is concerned, it is a reflection of how the materials are compressible or how much the density of the material decreases ($d\rho$) in effect

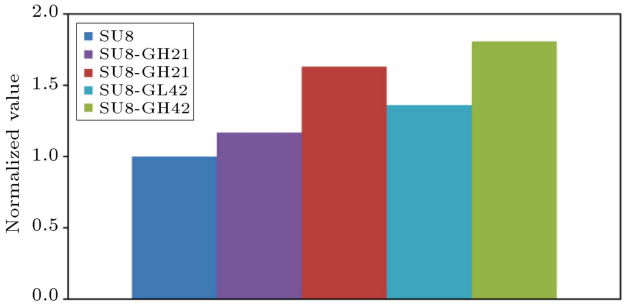

Figure 7. Average Young modulus of the compounds normalized with respect to the pure SU8.

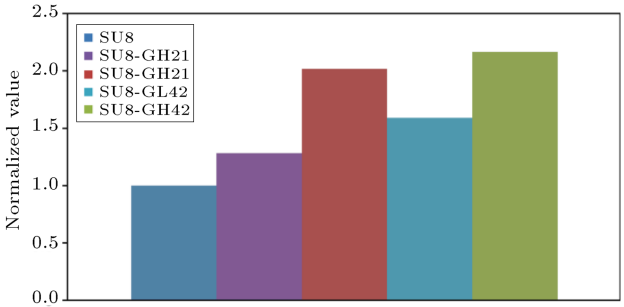

Figure 8. Average bulk modulus of the compounds with respect to the pure SU8.

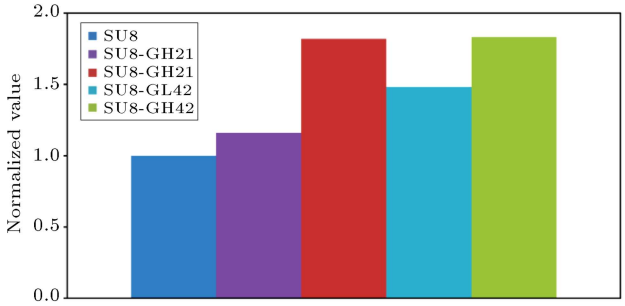

Figure 9. Average shear modulus of the compounds with respect to the pure SU8.

of an applied infinitesimal pressure (dP) described mathematically as in Eq. (7):

$$B = -V \times \left(\frac{\partial P}{\partial V}\right)_T, \tag{7}$$

or, in terms of density change:

$$B = \rho \times \left(\frac{\partial P}{\partial \rho}\right)_T. \tag{8}$$

Accordingly, the inverse of the bulk modulus is called compressibility β:

$$\beta = \frac{1}{B}. \tag{9}$$

The bulk compression involves only short-range conformational changes, whereas shear and tensile forces can cause strong (time-dependent) long-range conformational changes. Hence, the bulk modulus is the only time-independent modulus being a linear elastic property rather than viscoelastic one [46].

Therefore, the materials density is implicated in the bulk modulus of the nanocomposites: If the bulk modulus of the SU8-GL nanocomposites is lower than that of SU8-GH nanocomposites (Table 4, Figure 8), they are easily compressible, as compared to SU8-GH nanocomposites, due to less materials packing or lower density, showing lower relative mechanical properties expectedly.

Graphene deformation and wrinkling, discussed based on relative concentration profiles in the previous section, provide one with the wrinkled graphene layer which , of course, shows the lower mechanical reinforcement effect due to reduced interfacial interactions with the surrounding polymer.

4. Conclusion

In this work, the atomistic Molecular Dynamics (MD) simulation was used to simulate SU8 epoxy resin and its nanocomposites with graphene in order to investigate the effect of graphene on the mechanical properties of SU8. Two types of graphene layers were considered to determine the influence of the graphene aspect ratio. The interactions in simulated systems were calculated using LJ potential with a cutoff distance equal to 8 Å, and all simulation boxes had periodic boundary conditions in all directions. After energy minimization, the system was subjected to several steps of NPT run followed by several steps of NVT run at room temperature for equilibration and collection of the required data. Data showed that the low-aspect ratio graphene has a negative effect on the materials packing, leading to lower density. The mechanical properties estimated based on the constant strain approach elucidated that

the high-aspect ratio graphene leads to higher mechanical properties of the nanocomposites as a direct effect of higher density. Graphene wrinkling was observed in a low-aspect ratio containing nanocomposites which is, of course, an endorsement of the observed lower mechanical properties.

Acknowledgment

The authors wish to express their gratitude to Iran Nanotechnology Initiative Council for their partial financial support of the work under contract no. of 71734 and express their thanks for the support given by the Research and Technology Affair of the Sahand University of Technology without which the work could not have been accomplished successfully.

Nomenclature

U	Internal energy
C_{ij}	Elastic constants
σ	Stress
ε	Strain
λ, μ	Lame's constants
E	Young's modulus
B	Bulk modulus
G	Shear modulus
V	Volume
P	Pressure
P	Density
T	Temperature
B	Compressibility

References

1. Blagoi, G., Keller, S., Persson, F., Boisen, A., and Jakobsen, M.H. "Photochemical modification and patterning of SU-8 using anthraquinone photolinkers", *Langmuir*, **24**(18), pp. 9929-9932 (2008).
2. Hu, M., Guo, Q., Zhang, T., Zhou, S., and Yang, J. "SU-8-induced strong bonding of polymer ligands to flexible substrates via in situ cross-linked reaction for improved surface metallization and fast fabrication of high-quality flexible circuits", *ACS Appl. Mater. Inter.*, **8**(7), pp. 4280-4286 (2016).
3. Nagaiyanallur, V.V., Kumar, D., Rossi, A., Zürcher, S., and Spencer, N.D. "Tailoring SU-8 Surfaces: covalent attachment of polymers by means of nitrene insertion", *Langmuir*, **30**(33), pp. 10107-10111 (2014).
4. Rahiminejad, S., Pucci, E., Haasl, S., and Enoksson, P. "SU8 ridge-gap waveguide resonator", *Int. J. Microw. Wirel. T.*, **6**(05), pp. 459-465 (2014).
5. Rodríguez-Ruiz, I., Llobera, A., Vila-Planas, J., Johnson, D.W., Gómez-Morales, J., and García-Ruiz, J.M. "Analysis of the structural integrity of SU-8-based optofluidic systems for small-molecule crystallization studies", *Anal. Chem.*, **85**(20), pp. 9678-9685 (2013).
6. Romeo, A., Liu, Q., Suo, Z., and Lacour, S.P. "Elastomeric substrates with embedded stiff platforms for stretchable electronics", *Appl. Phys. Lett.*, **102**(13), pp. 131904 (2013).
7. Tian, Y., Shang, X., Wang, Y., and Lancaster, M.J. "Investigation of SU8 as a structural material for fabricating passive millimeter-wave and terahertz components", *J. Micro/Nanolithogr. MEMS. MOEMS.*, **14**(4), pp. 044507-044507-9 (2015).
8. Feng, R. and Farris, R. "The characterization of thermal and elastic constants for an epoxy photoresist SU8 coating", *J. Mater. Sci.*, **37**(22), pp. 4793-4799 (2002).
9. Mehboudi, A. and Yeom, J. "A two-step sealing-and-reinforcement SU8 bonding paradigm for the fabrication of shallow microchannels", *J. Micromech. Microeng.*, **28**(3), pp. 035002 (2018).
10. Ramanathan, T., Stankovich, S., Dikin, D., Liu, H., Shen, H., Nguyen, S., and Brinson, L. "Graphitic nanofillers in PMMA nanocomposites an investigation of particle size and dispersion and their influence on nanocomposite properties", *J. Polym. Sci. Poly. Phys.*, **45**(15), pp. 2097-2112 (2007).
11. Ramanathan, T., Abdala, A., Stankovich, S., Dikin, D., Herrera-Alonso, M., Piner, R., Adamson, D., Schniepp, H., Chen, X., and Ruoff, R. "Functionalized graphene sheets for polymer nanocomposites", *Nat. Nanotechnol.*, **3**(6), pp. 327-331 (2008).
12. George, J.J. and Bhowmick, A.K. "Ethylene vinyl acetate/expanded graphite nanocomposites by solution intercalation: preparation, characterization and properties", *J. Mater. Sci.*, **43**(2), pp. 702-708 (2008).
13. Villar-Rodil, S., Paredes, J.I., Martínez-Alonso, A., and Tascón, J.M. "Preparation of graphene dispersions and graphene-polymer composites in organic media", *J. Mater. Chem.*, **19**(22), pp. 3591-3593 (2009).
14. Duplock, E.J., Scheffler, M., and Lindan, P.J. "Hallmark of perfect graphene", *Phys. Rev. Lett.*, **92**(22), pp. 225502 (2004).
15. Schniepp, H.C., Li, J-L., McAllister, M.J., Sai, H., Herrera-Alonso, M., Adamson, D.H., Prud'homme, R.K., Car, R., Saville, D.A., and Aksay, I.A. "Functionalized single graphene sheets derived from splitting graphite oxide", *J. Phys. Chem. B*, **110**(17), pp. 8535-8539 (2006).
16. Geim, A.K. and Novoselov, K.S. "The rise of graphene", *Nat. Mater.*, **6**(3), pp. 183-191 (2007).
17. Szatkowski, P., Pielichowska, K., and Blazewicz, S. "Mechanical and thermal properties of carbon-nanotube-reinforced self-healing polyurethanes", *J. Mater. Sci.*, **52**(20), pp. 1-14 (2017).
18. Cai, D. and Song, M. "Recent advance in functionalized graphene/polymer nanocomposites", *J. Mater. Chem.*, **20**(37), pp. 7906-7915 (2010).

19. Ovid'Ko, I. "Enhanced mechanical properties of polymer –matrix nanocomposites reinforced by graphene inclusions: a review", *Rev. Adv. Mater. Sci.*, **34**(1), pp. 19-25 (2013).

20. Zeng, Q., Yu, A., and Lu, G. "Multiscale modeling and simulation of polymer nanocomposites", *Prog. Polym. Sci.*, **33**(2), pp. 191-269 (2008).

21. Rissanou, A.N. and Harmandaris, V. "Structure and dynamics of poly (methyl methacrylate)/graphene systems through atomistic molecular dynamics simulations", *J. Nanopart. Res.*, **15**(5), pp. 1589 (2013).

22. Rissanou, A.N. and Harmandaris, V. "Dynamics of various polymer-graphene interfacial systems through atomistic molecular dynamics simulations", *Matter.*, **10**(16), pp. 2876-2888 (2014).

23. Alian, A., Dewapriya, M., and Meguid, S. "Molecular dynamics study of the reinforcement effect of graphene in multilayered polymer nanocomposites", *Mater. Design*, **124**, pp. 47-57 (2017).

24. Güryel, S., Walker, M., Geerlings, P., De Proft, F., and Wilson, M. "Molecular dynamics simulations of the structure and the morphology of graphene/polymer nanocomposites", *Phys. Chem. Chem. Phys.*, **19**(20), pp. 12959-12969 (2017).

25. Sun, R., Li, L., Feng, C., Kitipornchai, S. and Yang, J. "Tensile behavior of polymer nanocomposite reinforced with graphene containing defects", *Eur. Polym. J.*, **98**, pp. 475-482 (2018).

26. Skountzos, E.N., Anastassiou, A., Mavrantzas, V.G., and Theodorou, D.N. "Determination of the mechanical properties of a poly (methyl methacrylate) nanocomposite with functionalized graphene sheets through detailed atomistic simulations", *Macromolecules*, **47**(22), pp. 8072-8088 (2014).

27. Ebrahimi, S., Ghafoori-Tabrizi, K., and Rafii-Tabar, H. "Multi-scale computational modelling of the mechanical behaviour of the chitosan biological polymer embedded with graphene and carbon nanotube", *Comp. Mater. Sci.*, **53**(1), pp. 347-353 (2012).

28. Rahman, R. and Haque, A. "Molecular modeling of crosslinked graphene-epoxy nanocomposites for characterization of elastic constants and interfacial properties", *Compos. Part B-Eng.*, **54**, pp. 353-364 (2013).

29. Theodorou, D.N. and Suter, U.W. "Atomistic modeling of mechanical properties of polymeric glasses", *Macromolecules*, **19**(1), pp. 139-154 (1986).

30. Rapold, R.F., Suter, U.W., and Theodorou, D.N. "Static atomistic modelling of the structure and ring dynamics of bulk amorphous polystyrene", *Macromol. Theory Simul.*, **3**(1), pp. 19-43 (1994).

31. Theodorou, D.N. and Suter, U.W. "Detailed molecular structure of a vinyl polymer glass", *Macromolecules*, **18**(7), pp. 1467-1478 (1985).

32. Zhang, J., Chan-Park, M.B., and Li, C.M. "Network properties and acid degradability of epoxy-based SU-8 resists containing reactive gamma-butyrolactone", *Sensor. Actuat. B-Chem.*, **131**(2), pp. 609-620 (2008).

33. Majidian, M., Grimaldi, C., Pisoni, A., Forró, L. and Magrez, A. "Electrical conduction of photopatternable SU8-graphene composites", *Carbon*, **80**, pp. 364-372 (2014).

34. Liu, Y., Zhang, C., Du, Z., and Li, H. "Preparation and curing kinetics of bisphenol A type novolac epoxy resins", *J. Appl. Polym. Sci.*, **99**(3), pp. 858-868 (2006).

35. Tam, L-h. and Lau, D. "Moisture effect on the mechanical and interfacial properties of epoxy-bonded material system: An atomistic and experimental investigation", *Polymer*, **57**, pp. 132-142 (2015).

36. Suter, M., Ergeneman, O., Zürcher, J., Moitzi, C., Pané, S., Rudin, T., Pratsinis, S., Nelson, B., and Hierold, C. "A photopatternable superparamagnetic nanocomposite: Material characterization and fabrication of microstructures", *Sensor. Actuat. B-Chem.*, **156**(1), pp. 433-443 (2011).

37. Hossenlopp, J., Jiang, L., Cernosek, R., and Josse, F. "Characterization of epoxy resin (SU-8) film using thickness-shear mode (TSM) resonator under various conditions", *J. Polym. Sci. Pol. Phys.*, **42**(12), pp. 2373-2384 (2004).

38. Tam, L-h. and Lau, D. "A molecular dynamics investigation on the cross-linking and physical properties of epoxy-based materials", *RSC Adv.*, **4**(62), pp. 33074-33081 (2014).

39. Shuichi, N. "Constant temperature molecular dynamics methods", *Prog. Theor. Phys. Supp.*, **103**, pp. 1-46 (1991).

40. Hoover, W.G. "Constant-pressure equations of motion", *Phys. Rev. A.*, **34**(3), pp. 2499-2500 (1986).

41. Verlet, L. "Computer experiments on classical fluids. I. Thermodynamical properties of Lennard-Jones molecules", *Phys. Rev.*, **159**(1), pp. 98-103 (1967).

42. Verlet, L. "Computer experiments on classical fluids. ii. Equilibrium correlation functions", *Phys. Rev.*, **165**(1), pp. 201-214 (1968).

43. Plimpton, S. Crozier, P., and Thompson, A. "LAMMPS-large-scale atomic/molecular massively parallel simulator", *Sandia National Laboratories*, **18** (2007).

44. Lin, F., Xiang, Y., and Shen, H-S. "Temperature dependent mechanical properties of graphene reinforced polymer nanocomposites-A molecular dynamics simulation", *Compos. Part B-Eng.*, **111**, pp. 261-269 (2017).

45. Ragab, T., McDonald, J., and Basaran, C. "Aspect ratio effect on shear modulus and ultimate shear strength of graphene nanoribbons", *Diam. Relat. Mater.*, **74**, pp. 9-15 (2017).

46. Seitz, J. "The estimation of mechanical properties of polymers from molecular structure", *J. Appl. Polym. Sci.*, **49**(8), pp. 1331-1351 (1993).

Biographies

Faraz Mohammadzadeh Honarvar is a last-year polymer engineering PhD student at Sahand University of Technology, Tabriz, Iran. He received a BS degree in Polymer Engineering from Amirkabir University of Technology (Tehran Polytechnic), Tehran, Iran and a MS degree in the same field from University of Tehran, Tehran, Iran. His research fields are nanocomposites, mechanical properties of nanocomposites and simulation of nanocomposites in molecular and macro scales. In addition, he is interested in a multi-scale simulation.

Behzad Pourabbas received his PhD in Polymer Science and Technology from University of Shira, Shiraz, Iran in 1996. He joined the Department of Chemical Engineering at Sahand University of Technology in Tabriz, Iran, as an Assistant Professor in that year, the institution in which he is still a member of the faculty. He promoted to Associate Professor Position in 2005 and to Full Professor Position in 2009. In 2008, when the Department of Polymer Engineering started its activity as an independent department, he joined and worked as the Head of the Department. During his academic career, he thought physical chemistry of polymers, polymer physics, polymer characterization methods and organic chemistry. His main research activities are focused on nanostructured materials, surface and surface modification, mono-microfabrication, conducting polymers and electronic materials. He has been the Research Vice-Chancellor of the University since 2016.

Mahdi Salami Hosseini obtained his BSc and MSc degrees from Amirkabir University of Technology in 2001 and 2004, respectively. He received his PhD in Polymer Engineering, from Amirkabir University of Technology, 2009. He joined Polymer Engineering Department at Sahand University of Technology as an Assistant Professor in 2009 and became an Associate Professor in 2015. His current research interests include process simulation and numerical rheology using Finite-Element Method (FEM) and Stokesian Dynamics (SD) focusing on microfluidic devices.

Mahsa Kharazi received her PhD degree in Aerospace Engineering from Amirkabir University of Technology (Tehran Polytechnic), Tehran, Iran, in 2008. She joined the Department of Mechanical Engineering at Sahand University of Technology, Tabriz, Iran, as an Assistant Professor, and as a faculty member in 2008. She became an Associate Professor, in the same department in 2017. Her teaching areas are continuum mechanics, plasticity, finite-element method, and stability of structures. Her PhD thesis was on the stability analysis of delaminated composite materials and, over the last five years, she has become involved in damage modeling and analysis in solid mechanics. Her current research interests include structural stability, damage analysis, numerical methods, and non-local theories.

Hamid Erfan-Niya received the PhD degree in Chemical Engineering, in 2011, from Amirkabir University of Technology (Tehran Polytechnic), Tehran, Iran. He is currently an Assistant Professor of Chemical Engineering at University of Tabriz, Tabriz, Iran. His research interests are molecular simulation of nanoscale phenomena. In addition, he works on interfacial phenomena, membrane-based water desalination, and gas separation systems. His published articles are related to the subjects including gas hydrates, nanofluids, nanocomposites, water desalination, and drug delivery systems.